JOURNAL OF CATALYSIS 157, 713–720 (1995)

# Structure and Catalytic Property of Coherent Spinel Surface Layers on Hexaaluminate Microcrystals

Masato Machida,* Akihiro Sato,* Manabu Murakami,* Tsuyoshi Kijima,* and Hiromichi Arai†

*Department of Materials Science, Faculty of Engineering, Miyazaki University, Gakuen Kibanadai Nishi 1-1, Miyazaki 889-21, Japan; and †Department of Materials Science, Graduate School of Engineering Sciences, Kyushu University, Kasugakoen 6-1, Kasuga, Fukuoka 816, Japan

Received May 30, 1995; revised August 15, 1995; accepted August 21, 1995

**Formation of coherent surface layers of $Mn_3O_4$ on hexaaluminate microcrystals has been studied as a structural modification to enhance the catalytic activity for methane combustion. The spinel oxide surface layer was successfully produced on planar microcrystals of hexaaluminate by employing the air oxidation of an aqueous Mn(II) solution. As evident from TEM, XPS, and $CO_2$ chemisorption measurements, as-prepared surface layers completely covered the basal plane of planar microcrystals. This characteristic structure appears to be a result of liquid phase epitaxy at the structurally coherent interface between hexaaluminate and spinel. A completely different structure was observed for the samples from the conventional impregnation method, which contain insular $Mn_3O_4$ particles dispersed on hexaaluminate. The catalytic activity for methane combustion was evaluated as a function of the $Mn_3O_4$ loading and the metal composition of the spinel surface layer. It was revealed that the higher specific activity was observed over air-oxidation-derived samples than over the impregnated samples. Partial substitution of Fe for Mn on the surface layer was effective in enhancing the combustion activity as a result of promoting the reduction/oxidation property.** 

## INTRODUCTION

We have previously developed the Mn-substituted hexaaluminates ($BaMn_xAl_{12-x}O_{19}$) for a high-temperature catalytic combustion (1–3). This novel catalyst is characterized by not only the excellent thermal stability above 1000°C but also the high activity for methane combustion. The specific surface area was retained above 20 $m^2/g$ even upon heating at 1300°C, at which conventional alumina-supported catalysts sinter into nonporous agglomerates with surface areas less than 5 $m^2/g$. This thermal stability is related to the unique crystal structure, consisting of the alternative stacking of a spinel block and a monatomic layer with large cations such as Ba or La (4–6). Retention of the large surface area is closely related to the very thin planar morphology of the hexaaluminate microcrystal, which is reflected by the layered structure. The catalytic activity of Mn-substituted hexaaluminates is dependent on the concentration of manganese ions, which occupy the tetragonal Al site in the spinel block (7). However, increasing the amount of Mn substitution ($x > 3$ in $BaMn_xAl_{12-x}O_{19}$) brings about deterioration of the hexaaluminate phase, accompanied by a significant loss of surface area (1). Therefore, alternative structural modification is necessary to improve the catalytic activity of Mn-substituted hexaaluminates.

In this study, we noted the formation of surface layers on hexaaluminate microcrystals as one promising modification to enhance the catalytic activity. Fortunately, planar particles of hexaaluminate possess extremely flat surfaces on the basal plane, which are suitable for the epitaxial crystal growth of metal oxide. The resultant surface layers are expected to produce interesting catalytic activity as a result of the combination with hexaaluminate. In particular, several spinel oxides ($Mn_3O_4$, $Co_3O_4$, $Fe_3O_4$, etc.) are quite interesting, because their structural similarity to hexaaluminates might lead to strong interactions at the interface. Furthermore, these materials are convenient to use as surface modifiers because the liquid phase deposition is applicable (8–10). The structure and catalytic properties of surface modified hexaaluminates have been characterized in comparison with conventional impregnated catalysts.

## METHODS

### *Preparation of Sample*

Barium hexaaluminate ($Ba_{0.75}Al_{11}O_{17.25}$) and its Mn-substituted sample ($Ba_{0.75}MnAl_{10}O_{17.25}$) were prepared by calcining the hydrolyzed metal alkoxides at 1100°C as described in previous manuscripts (1, 2). The metallic composition of hexaaluminate is determined on the basis of single crystal structural studies of Ba hexaaluminate, which were conducted by Iyi *et al.* (11).

Supported manganese oxide samples, $Mn_3O_4/Ba_{0.75}MAl_{10}O_{17.25}$, ($M$ = Al, Mn) were prepared by an air-oxidation process (8–10). Hexaaluminate powders and



0021-9517/95 $12.00

manganese nitrate were added to ion-exchanged water which was deoxidized by $N_2$ bubbling overnight. The resultant suspension was vigorously stirred under an $N_2$ atmosphere and air oxidation was performed by passing air bubbles through the solution at 70°C and pH ca.7. The spinel formation in the air-oxidation process results from the reaction (9)

$$2MnOH^{2+} + MnOH^{+} + OH^{-} \rightarrow Mn^{2+}Mn_2^{3+}O_4 + 4H^{+}.$$

According to this oxidation process, the hydroxide ion species of Mn, adsorbing onto hexaaluminate microcrystals, are deposited as spinel oxides to produce the surface layer. The contamination due to unreacted nitrates or hydroxides was removed by soaking the powder product with a dilute hydrochloric acid. For the preparation of surface layers consisting of partially substituted $Mn_3O_4$ ($(Mn_{1-x}M_x)_3O_4$, $M$ = Fe, Co, Ni) mixed nitrate solutions were submitted to the air-oxidation process. The $Mn_3O_4$/hexaaluminate samples were also obtained from the conventional impregnation method. Hexaaluminate powders were suspended in an aqueous solution of $Mn(NO_3)_2$ followed by evaporation to dryness. The dried sample was calcined at 500°C in air to decompose the nitrate to manganese oxide.

*Characterization*

The crystal structure of hexaaluminate supported $Mn_3O_4$ samples was determined by powder X-ray diffraction (XRD, Rigaku RINT1400) with Cu$K_\alpha$ radiation. The specific surface area was measured by the BET method using nitrogen adsorption. A transmission electron microscope (JEOL, JEM-4000EX, 400 keV) was used for imaging and electron diffraction (ED) of the $Mn_3O_4$/hexaaluminate interface structure.

Carbon dioxide chemisorption was carried out to study the surface structure of $Mn_3O_4$ supported on hexaaluminate microcrystals. Carbon dioxide is known to bring about strong chemisorption onto metal species with basic character. For instance, Bettmann *et al.* (12) evaluated the dispersion of La ions on the surface of alumina by means of $CO_2$ chemisorption. In the case of the present study, the irreversible $CO_2$ chemisorption occurs dominantly onto Ba species exposed to the surface but negligibly onto $Mn_3O_4$. Therefore, amounts of $CO_2$ chemisorption will reflect the surface coverage of hexaaluminate microcrystals. Adsorption isotherms of $CO_2$ were measured in a conventional volumetric vacuum system at room temperature. After evacuating the sample at 500°C, incremental $CO_2$ uptake at increasing pressures was measured with a pressure sensor. This first measurement was followed by evacuation at room temperature to remove reversibly adsorbed $CO_2$. Then, the $CO_2$ adsorption measurement was repeated to obtain the reversible adsorption isotherm. The amount of irreversible $CO_2$ chemisorption was determined from the difference of a pair of these adsorption isotherms.

The surface analysis of $Mn_3O_4$/hexaaluminate samples was carried out by XPS spectrometer (VG, Escascope) using Mg$K_\alpha$ radiation (15 kV, 20 mA). The powdered sample pressed into a disk was loaded into the spectrometer and evacuated at room temperature overnight prior to the XPS measurement. During analysis, the background pressure was maintained below $10^{-6}$ Pa.

Temperature programmed desorption (TPD) of oxygen was measured to evaluate the redox property of the sample. Prior to the measurement, the sample was treated under an oxygen stream at 500°C for 1 h; this was followed by cooling to room temperature. After evacuation, the sample was heated at a constant rate of 10°/min under a He stream (50 ml/min). The desorbed oxygen in the effluent gas was detected with a TCD cell.

*Measurement of $CH_4$ Combustion Activity*

Catalytic activity of supported $Mn_3O_4$ samples was measured in a conventional flow system at atmospheric pressure. Catalysts (1.0 g) were fixed in a quartz tube (6 mm i.d.) by packing a quartz wool at both ends of the catalyst bed. A gaseous mixture of methane (2 vol%) and air (98 vol%) was fed to the catalyst bed at $W/F$ = 0.01 g-cat min/cm$^3$. The methane conversion in the effluent gas was analyzed by on-line gas chromatography with molecular sieve and Porapack-Q columns.

## RESULT AND DISCUSSION

*Formation and Structure of Spinel Surface Layers on Hexaaluminate*

Figure 1 shows the XRD patterns of $Mn_3O_4$/hexaaluminates prepared by air oxidation and conventional impregnation. The neat samples corresponding to the composition $Ba_{0.75}Al_{11}O_{17.25}$ or $Ba_{0.75}MnAl_{10}O_{17.25}$ were composed of a single phase of hexaaluminate after calcination at 1100°C. When the $Mn_3O_4/Ba_{0.75}MnAl_{10}O_{17.25}$ was prepared from conventional impregnation and subsequent calcination at 500°C, the diffraction pattern of hexaaluminate was unchanged and the formation of a spinel $Mn_3O_4$ phase was observed above 10 wt% of the loading.

In contrast, the XRD patterns exhibited by the sample from air oxidation are completely identical to that of hexaaluminate at a loading amount of $Mn_3O_4$ of less than 30 wt%. The reflections of the $Mn_3O_4$ phase can be observed only above 30 wt% of the loading. The difference of diffraction patterns between samples from these two preparation routes is considered to be associated with the microstructure of supported $Mn_3O_4$. The impregnation and subsequent calcination produces the independent

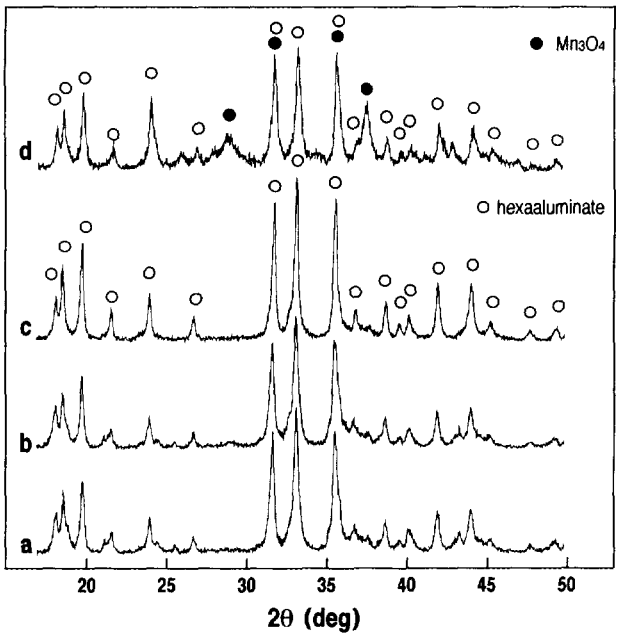


FIG. 1. XRD patterns of (a) 5 wt%, (b) 8 wt%, (c) 10 wt% $Mn_3O_4$/$Ba_{0.75}MnAl_{10}O_{17.25}$ prepared by air oxidation and (d) 10 wt% $Mn_3O_4$/$Ba_{0.75}MnAl_{10}O_{17.25}$ prepared by conventional impregnation.

particles of manganese oxide, which are supported onto hexaaluminate. In the air-oxidation process, however, the spinel is directly deposited onto hexaaluminate from solutions.

According to a previous study by Abe and Tamaura (9), the spinel formation in the air-oxidation process occurs between manganese hydroxide cations in the presence of base as described in the Methods section. The manganese hydroxide cations with different oxidation numbers ($Mn^{3+}$ and $Mn^{2+}$) adsorb onto the surface of hexaaluminates and subsequent deprotonation produces the $Mn^{2+}$–O–$Mn^{3+}$ bonds. By repetition of the adsorption and deprotonation processes, the formation of spinel surface layer proceeds continuously on the surface of hexaaluminate microcrystals. When the air oxidation of Mn(II) was performed in the absence of hexaaluminate powders, the product was a single phase of spinel $Mn_3O_4$ with the BET surface area of 24 $m^2/g$.

Since the XRD measurement was not conclusive on the structure of the sample from air oxidation, further microstructural analysis was carried out by a transmission electron microscope to obtain the direct image of the supported structure. Figure 2 shows TEM photographs and ED patterns of 10 wt% $Mn_3O_4/Ba_{0.75}MnAl_{10}O_{17.25}$ powders prepared from air oxidation. As shown in Fig. 2a, the sample consisted of highly dispersed planar crystallites 100–200 nm in diameter and 20–40 nm thick. The planar particles have an orientation parallel to the (001) plane of the hexaaluminate structure. Figure 2b shows the structural image in the vicinity of the basal plane surface of hexaaluminate facets (incident beam normal to (120)). The image apparently demonstrates the appearance of surface layers of ca. 4-nm thick parallel to the layer structure. While hexaaluminate is characterized by an array of layers of 1.1-nm thick along [001], the surface layer contains contours of 0.5-nm thick, which agree with $d_{110}$ of $Mn_3O_4$ with a tetragonal unit cell. The electron diffraction of this interface region taken from the [$\bar{1}$20] zone axis (Fig. 2c) shows weak extra reflection rows just parallel to the [00$l$] direction (noted by arrows). These rows correlate to the existence of the surface layer, the alignment of which suggests the coherent interface structure as discussed below. Although the surface layers almost completely covered the basal plane of hexaaluminate, the deposition on the side plane of planar particles was not clear from TEM images.

*Surface Coverage of Spinel/Hexaaluminate*

Carbon dioxide adsorption takes place strongly onto Ba species exposed to the surface of hexaaluminate, but negligibly onto $Mn_3O_4$ layers covering the surface of hexaaluminate. Therefore, the surface coverage for $Mn_3O_4$/hexaaluminate samples can be estimated by measuring irreversible $CO_2$ adsorption, which is plotted as a function of the loading amount of $Mn_3O_4$ in Fig. 3. The $CO_2$ chemisorption for the sample from air oxidation steeply decreased to zero with increased $Mn_3O_4$ loading, showing that the $Mn_3O_4$ completely covered the surface Ba site at 5 wt% of loading. Although the surface distribution of Ba ions on hexaaluminates is not clear because of the different crystal planes exposed, we assume that they should be exposed mainly on the basal plane surface of the microcrystal, (001), which is just parallel to the array of $Ba^{2+}$ ions. The difference of $CO_2$ chemisorption between $Ba_{0.75}Al_{11}O_{17.25}$ and $Ba_{0.75}MnAl_{10}O_{17.25}$ probably results from the differences of aspect ratio of the planar microcrystals or the Ba concentration on the basal plane surface. Figure 3 evidences the formation of $Mn_3O_4$ surface layers which completely cover the basal plane surface of hexaaluminate microcrystals.

From the critical loading amount of $Mn_3O_4$ (ca. 5 wt%), the corresponding thickness of the surface layers was estimated as follows. For this calculation, the shape of the hexaaluminate ($Ba_{0.75}Al_{11}O_{17.25}$) crystallite was assumed to be a right circle cylinder, of which the basal plane is parallel to the (001) face. Statical geometry of this crystallite was obtained by applying the line broadening analysis of (00$l$) and ($hk$0) X-ray diffraction peaks. To correct the instrumental broadening for each diffraction peak, the whole pattern profile decomposition (WPPD) method, developed by Toraya (12, 13), was adopted and the result shows dimensions of 110 nm in diameter and 28 nm in thickness. This means that 67% of the geometrical surface

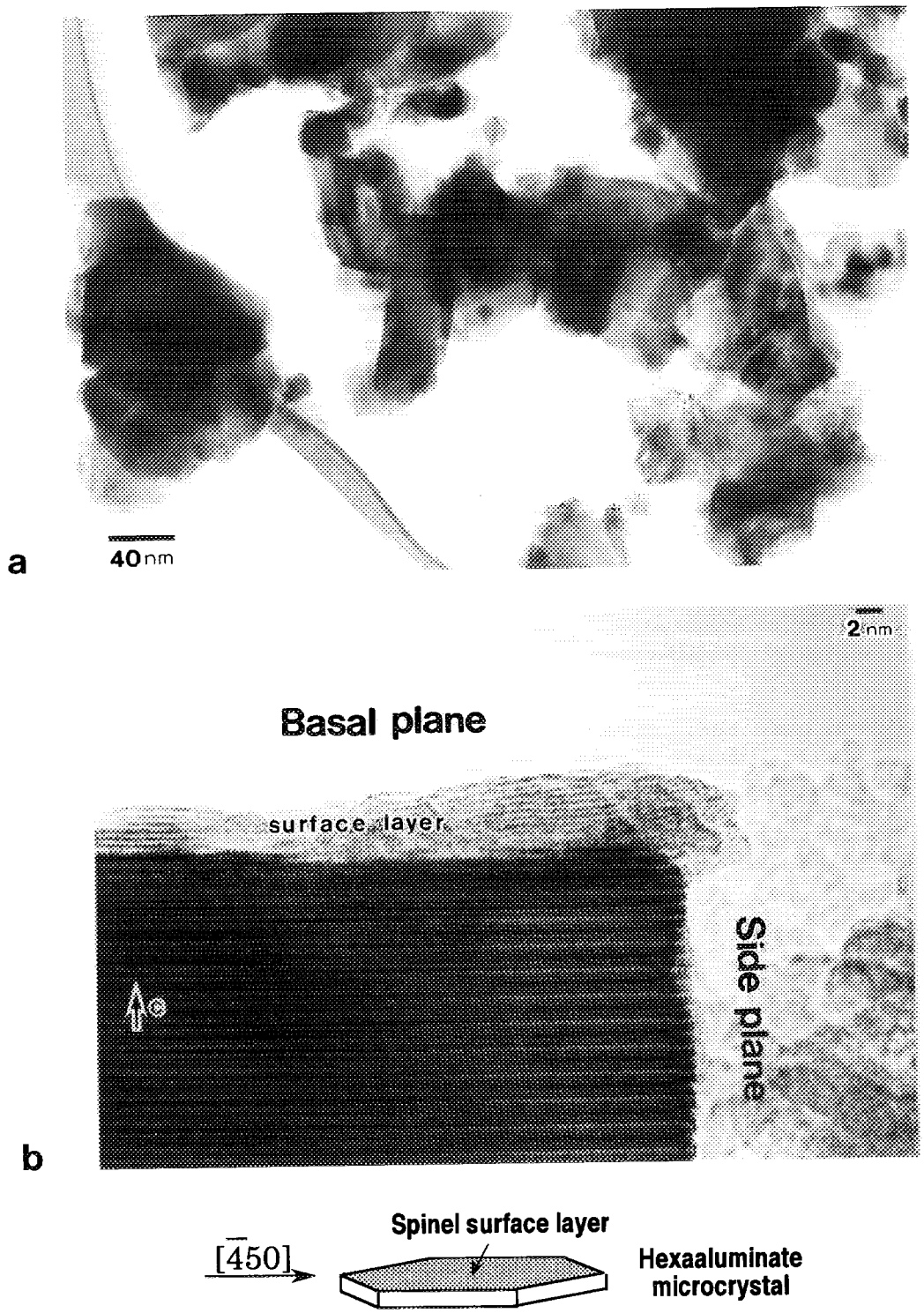


FIG. 2. TEM photographs of 10 wt% $Mn_3O_4/Ba_{0.75}MnAl_{10}O_{17.25}$ prepared by air oxidation. (a) Low magnification image of as-prepared powders. (b) Structural image of a spinel surface layer deposited on the basal plane of hexaaluminate (incident beam parallel to [450] of hexaaluminate). (c) Corresponding electron diffraction taken from the spinel/hexaaluminate interface and a calculated pattern of hexaaluminate.

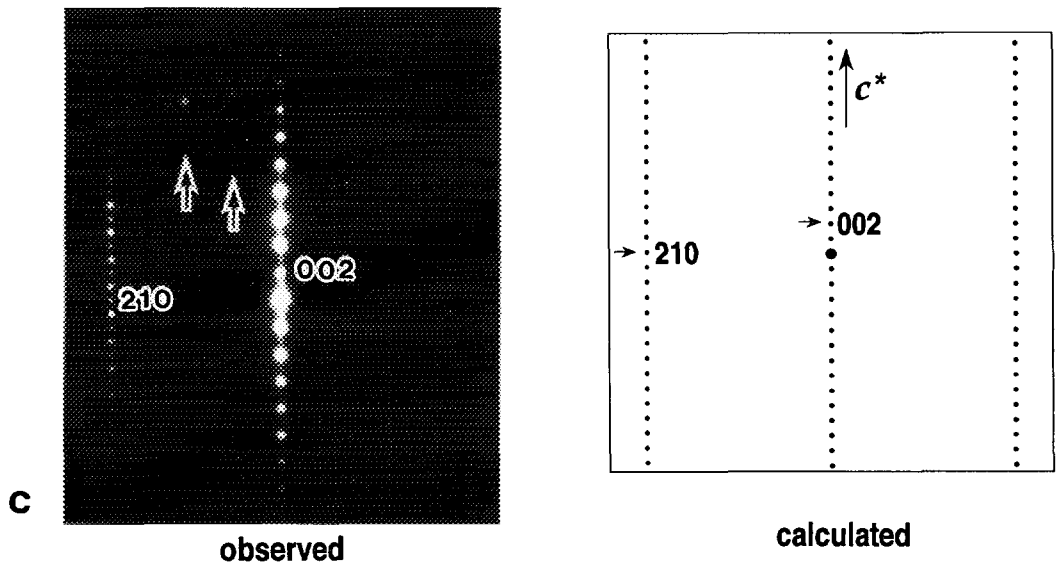


FIG. 2—*Continued*

area, which corresponds to 13 $m^2/g$ of the BET surface area, should be attributed to the basal plane of the planar crystallites. This surface area of the basal plane is very close to the value ca. 10 $m^2/g$ which was estimated from the irreversible $CO_2$ adsorption under the assumption that the $CO_2$/Ba ratio was equal to unity. Consequently, the complete coverage of basal planes by 5 wt% loading of $Mn_3O_4$ requires the mean thickness of the surface layer to be ca. 0.8 nm. These considerations conclude that the $Mn_3O_4$ surface layer can completely cover the basal plane even in the form of a two-dimensional monolayer invisible by TEM and/or XRD.

Figure 3 also shows the amount of $CO_2$ chemisorbed onto the impregnated $Mn_3O_4$/hexaaluminates. For the impregnated sample, however, a substantial amount of $CO_2$ chemisorption was observed even after the loading of 10 wt% $Mn_3O_4$. The result is consistent with the microstructure consisting of insularly dispersed $Mn_3O_4$ particles on hexaaluminate microcrystals. The complete coverage by surface layers of spinel $Mn_3O_4$ cannot be attained by a conventional impregnation process.

As revealed in TEM observation, the thickness of 10 wt% $Mn_3O_4$ surface layers on the basal plane of hexaaluminate microcrystals is about 4 nm, which seems larger than the escape depth of photoelectrons. Thus, XPS spectra should demonstrate the difference in surface coverage of hexaaluminate microcrystals. Figure 4 shows the typical XPS spectra of $Mn_3O_4/Ba_{0.75}MnAl_{10}O_{17.25}$ samples prepared from impregnation or air oxidation. A neat sample of $Ba_{0.75}MnAl_{10}O_{17.25}$ represents strong Ba 3*d* (796 and 781 eV) and weak Mn 2*p* (652 and 641 eV) signals. Since the sample consists of single phase of hexaaluminate, the intensity of both signals represents the surface composition of Mn-substituted hexaaluminate. The impregnation of $Mn_3O_4$ increased the intensity of Mn 2*p* and, in contrast, decreased that of the Ba 3*d* signals. This indicates the deposition of $Mn_3O_4$ particles on the planar particles of hexaaluminates, but the Ba 3*d* signals remained strong even after deposition of 20 wt% $Mn_3O_4$. A similar change of XPS spectra was obtained for the samples from the air-oxidation process. As compared to the impregnated samples, however, the Ba 3*d* signals were much weaker even after loading of 5 wt% $Mn_3O_4$. In addition, relatively strong Mn 2*p* signals indicate high surface coverage of $Mn_3O_4$. These XPS results are consistent with the result

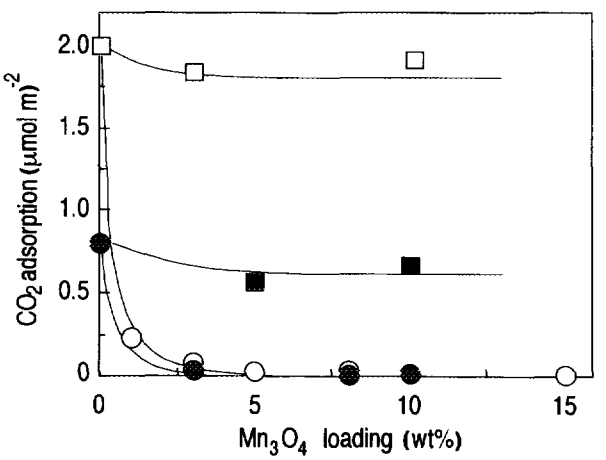


FIG. 3. Amounts of irreversible $CO_2$ adsorption onto $Mn_3O_4$/hexaaluminate as a function of the loading amount of $Mn_3O_4$ (25°C). ○, $Mn_3O_4/Ba_{0.75}Al_{11}O_{17.25}$ (air oxidation); ●, $Mn_3O_4/Ba_{0.75}MnAl_{10}O_{17.25}$ (air oxidation); □, $Mn_3O_4/Ba_{0.75}Al_{11}O_{17.25}$ (impregnation); ■, $Mn_3O_4/Ba_{0.75}MnAl_{10}O_{17.25}$ (impregnation).

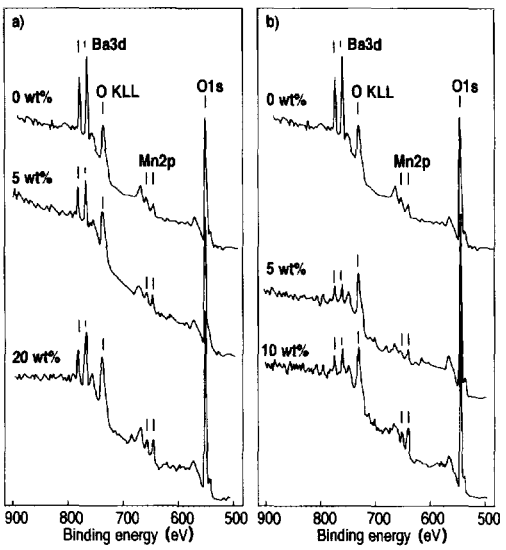


FIG. 4. XPS spectra of $Mn_3O_4/Ba_{0.75}MnAl_{10}O_{17.25}$ with various $Mn_3O_4$ loadings. Samples were prepared by (a) conventional impregnation and (b) the air-oxidation process.

of $CO_2$ chemisorption and TEM images of spinel/hexaaluminate.

*Interface Structure of Spinel/Hexaaluminate*

Experimental results presented in the previous sections conclude that the surface spinal layer was produced on hexaaluminate microcrystals when prepared from the air-oxidation process. One of the reasons why such surface layers form is the structural coherence between spinel and hexaaluminate. An ideal spinel structure consists of cubic close-packed array of oxide ions in which metallic ions occupy 1/8 of tetrahedral sites and 1/2 the octahedral sites (14). Although the unit cell of $Mn_3O_4$ is distorted into a tetragonal structure ($a$ = 0.807 nm, $c$ = 0.943 nm), the ionic configuration is on the basis of spinel structure (15, 16). On the other hand, Ba–hexaaluminate can be considered as a hexagonal $\beta$-alumina structure, which is made up of cubic close packed blocks, four layers of oxygen ions thick, in which the aluminum ions occupy both the tetrahedral and octahedral positions (17). Obviously, ionic configuration in this part of $\beta$-alumina are very similar to that of a spinel structure.

It should be noted that there exists an oriented relationship between the surface layer and hexaaluminate as evident from the ED pattern taken from the interface region (Fig. 2c). The surface layer, showing a periodicity along the $c$ axis of hexaaluminate, demonstrates the formation of a coherent interface. A structural model for the interface could thus be proposed as shown in Fig. 5, which represents the projection on (4$\bar{5}$0) of hexaaluminate. The basal plane surface of hexaaluminate corresponds to (001), being the interface between the two phases. Although the hexaaluminate structure is terminated by a mirror plane on the basal plane surface, the common ionic arrangement of both phases results in a continuous coherent interface by sharing $Ba^{2+}$ and $O^{2-}$ ions.

According to this structural model, the $Mn_3O_4$/hexaaluminate interface can be considered as the epitaxial growth of a spinel lattice on the (001) surface of hexaaluminate. The air-oxidation process seems effective in promoting the formation of this type of interface structure because it allows continuous growth of spinel lattices from a liquid phase. On the other hand, the surface layer was not visible at all on the side plane surface of hexaaluminate microcrystals (Fig. 2b). The side plane almost perpendicular to (001) exposes spinel blocks separated each other by the mirror plane. Therefore, the spinel/hexaaluminate interface is so unstable due to a large misfit that coherency between the two phases is frustrated. This is likely the reason why the coherent surface layer cannot be set up on the side plane of hexaaluminate microcrystals.

*Methane Combustion Activity of Spinel/Hexaaluminate*

Catalytic activity of $Mn_3O_4$/hexaaluminates for methane oxidation was evaluated in a conventional fixed bed reactor. Figure 6 shows the methane conversion into $CO_2$ (400°C) over $Mn_3O_4/Ba_{0.75}MnAl_{10}O_{17.25}$ prepared by air oxidation as well as by impregnation. The methane conversion over unsupported $Mn_3O_4$ is 21.5%, which corresponds to $1.92 \times 10^{-5}$ mol/min · g-$Mn_3O_4$ of reaction rate. The catalytic activity of impregnated samples calcined at 500°C increased monotonically with a loading amount of $Mn_3O_4$. This is in contrast to the air-oxidation-derived sample, which retained high activity even at a low loading amount.

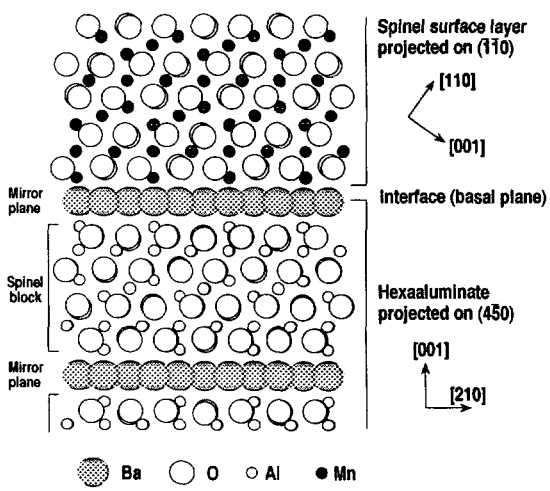


FIG. 5. A model for spinel/hexaaluminate with coherent interface structure.

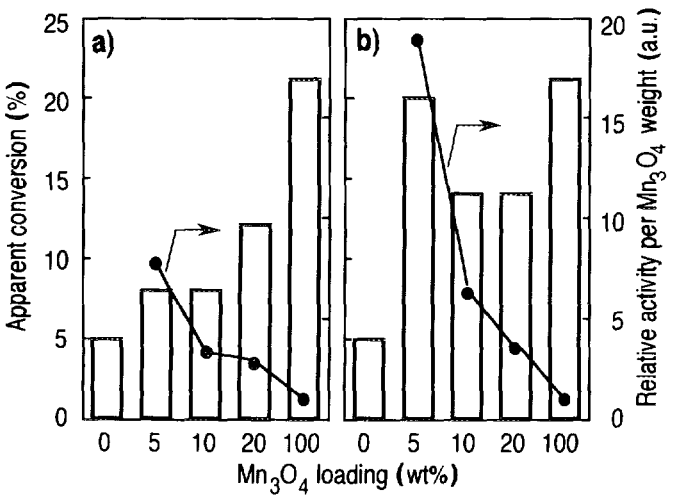


FIG. 6. Methane combustion activity of $Mn_3O_4/Ba_{0.75}MnAl_{10}O_{17.25}$ as a function of the loading amount of $Mn_3O_4$ (400°C). Catalysts were prepared by (a) impregnation and (b) the air-oxidation process. Reaction conditions: $CH_4$ 2 vol%, air 98 vol%, $W/F$ = 0.01 g-cat. min cm$^{-3}$.

Figure 6 also shows the specific catalytic activity per unit $Mn_3O_4$ loading, which is normalized by the activity of unsupported $Mn_3O_4$. It is noted that higher specific activity was attained for the air-oxidation-derived sample at the lower amount of $Mn_3O_4$ loading. This result coincides with the difference of surface microstructure of both samples. High surface coverage of hexaaluminate microcrystals by $Mn_3O_4$ is effective in promoting catalytic reaction in accord with the abundant active sites. However, the preparation by impregnation does not attain the high surface coverage because of agglomeration of the insularly dispersed $Mn_3O_4$ particles.

*Effect of Partial Substitution in Spinel Surface Layer*

The effect of partial substitution for Mn in the spinel layers was next examined to enhance the catalytic activity of $Mn_3O_4$/hexaaluminate. The mixed spinel surface layers ($(Mn_{1-x}M_x)_3O_4$, $M$ = Fe, Co, and Ni) were produced on $Ba_{0.75}MnAl_{10}O_{17.25}$ by the air-oxidation process. Among these systems, spinel solid solutions are available in the whole compositional range in $(Mn_{1-x}Fe_x)_3O_4$, but limited at $x < 0.3$ in $(Mn_{1-x}Ni_x)_3O_4$ (18, 19).

Their catalytic activities for methane combustion are summarized in Fig. 7 as a function of $x$ in $(Mn_{1-x}M_x)_3O_4$. The combustion activity is expressed as temperatures $T_{10\%}$ and $T_{90\%}$, at which methane conversions to $CO_2$ of 10 and 90%, respectively, were attained. Apparently, Ni substitution was not effective in improving the activity. This is partially because of incomplete coverage of hexaaluminate in this system. In the $(Mn_{1-x}Co_x)_3O_4$ system, however, an increase in the activity was observed at $x \approx$

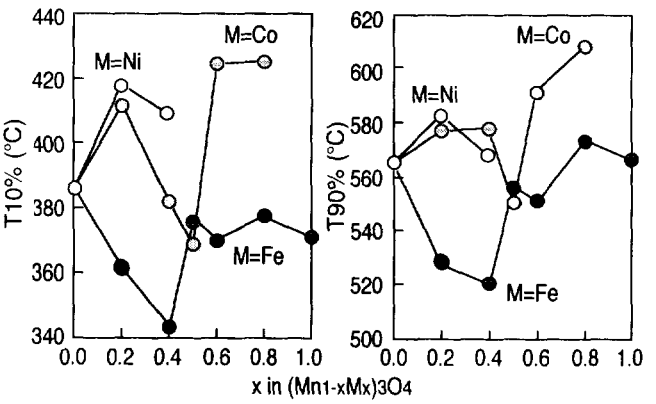


FIG. 7. Methane combustion activity of $(Mn_{1-x}M_x)_3O_4$($M$ = Fe, Co, and Ni)/$Ba_{0.75}MnAl_{10}O_{17.25}$ prepared by air oxidation. $T_{10\%}$ and $T_{90\%}$ are the temperatures at which methane conversion to $CO_2$ reached 10 and 90%, respectively. Reaction conditions: see legend of Fig. 6.

0.4. Partial substitution by Fe attained the most prominent effect in promoting the catalytic activity over a wide range of composition. The maximum activity was obtained at $x \approx 0.4$, corresponding to the formation of $FeMn_2O_4$. This system produced spinel layers with the complete surface coverage as evident from the $CO_2$ chemisorption measurement, because the solid solution can be obtained easily.

To clarify the effect of the partial substitution of spinel surface layers, the reduction–oxidation property was studied by means of TPD of $O_2$. As can be seen in Fig. 8,

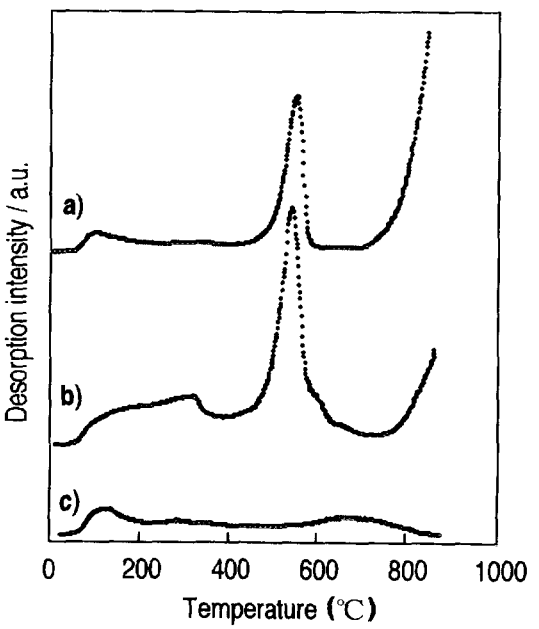


FIG. 8. TPD profiles of oxygen from substituted spinel oxides, $(Mn_{1-x}Fe_x)_3O_4$. (a) $x$ = 0, (b) $x$ = 0.4, and (c) $x$ = 1.0.

unsubstituted $Mn_3O_4$ showed three types of desorption peaks at <200, 550, and <750°C. The large desorption peak at <750°C is due to reduction of bulk $Mn_3O_4$ and the other low-temperature peaks are associated with nonstoichiometry and/or weakly-adsorbed oxygen species. In particular, a sharp $O_2$ desorption peak at 550°C, considered to be ascribable to excess bulk oxygens due to the cation-deficient character of $Mn_3O_4$, should come into play in catalytic reactions. This is supported by the initiation temperature of methane oxidation in accord to that of the low-temperature $O_2$ desorption. The oxygen desorption at low temperatures increased with partial substitution of Fe for Mn, being consistent with the increased catalytic activity of this system (Fig. 7). Although the oxygen desorption from a $Fe_3O_4$ sample was extremely small in accordance with the stability against the reduction, Fe-substitution appears effective in promoting the reduction/oxidation of Mn species. A typical inverse spinel, $Fe_3O_4$, contains a half of $Fe^{3+}$ in the tetrahedral site, which is occupied by $Mn^{2+}$ in a normal spinel, $Mn_3O_4$. In the $FeMn_2O_4$ structure, however, the cation distribution is intermediate between those of normal and inverse spinels, i.e., both divalent ($Fe^{2+}$, $Mn^{2+}$) and trivalent ($Fe^{3+}$, $Mn^{3+}$) cations distribute between tetragonal and octahedral sites (20). Thus, one reason for the increase of the $O_2$ desorption will be related to charge transfer due to a mixed valence on each cation site. Consequently, accelerating redox cycles must be more favorable for catalytic oxidation of methane. The partial substitution of metallic elements in spinel surface layers is one of the easiest and most effective methods to increase the catalytic activity.

## ACKNOWLEDGMENT

This study was supported by Iketani Science and Technology Foundation and the Association for the Progress of New Chemistry.

## REFERENCES

1. Machida, M., Eguchi, K., and Arai, H., *J. Catal.* **120,** 386 (1989).
2. Machida, M., Eguchi, K., and Arai, H., *J. Catal.* **123,** 477 (1990).
3. Sekizawa, K., Machida, M., Eguchi, K., and Arai, H., *J. Catal.* **142,** 655 (1993).
4. Machida, M., Eguchi, K., and Arai, H., *J. Catal.* **103,** 385 (1987).
5. Machida, M., Eguchi, K., and Arai, H., *Bull. Chem. Soc. Jpn.* **61,** 3659 (1987).
6. Machida, M., Eguchi, K., and Arai, H., *J. Am. Ceram. Soc.* **71,** 1142 (1988).
7. Machida, M., Inoue, H., Shiomitsu, T., Eguchi, K., and Arai, H., *Ceram. Trans. Ser.* **31,** 273 (1992).
8. Kiyama, M., *Bull. Chem. Soc. Jpn.* **47,** 1646 (1974).
9. Abe, M., and Tamaura, Y., *Jpn. J. Appl. Phys.* **22,** L511 (1983).
10. Aoki, N., *Bull. Ceram. Soc. Jpn.* **26,** 195 (1991).
11. Iyi, N., Inoue, Z., Takekawa, S., and Kimura, S., *J. Solid State Chem.* **52,** 66 (1984).
12. Bettman, M., Chase, R. E., Otto, K., and Weber, W. H., *J. Catal.* **117,** 447 (1989).
13. Toraya, H., *J. Appl. Crystallogr.* **21,** 192 (1988).
14. Galasso, F. S., "Structure and Properties of Inorganic Solids" p. 239. Pergamon, Elmsford, NY, 1970.
15. Bacon, G. E., and Roberts, F. F., *Acta. Crystallogr.* **6,** 57 (1953).
16. Wickham, D. G., and Croft, W. J., *Phys. Chem. Solids* **7,** 351 (1958).
17. Iyi, N., Takekawa, S., and Kimura, S., *J. Solid State Chem.* **83,** 8 (1989).
18. van Hook, H. J., and Keith, M. L., *Am. Mineral.* **43,** 80 (1958).
19. Zacharias, H. J., *Phys. Status Solidi A* **22,** K85 (1974).
20. Sinah, A. P. B., Sinjana, W. R., and Biswas, A. B., *Acta. Crystallogr.* **10,** 439 (1957).